INTERNATIONAL JOURNAL OF HYDROGEN ENERGY XXX (XXXX) XXX

Available online at www.sciencedirect.com

ScienceDirect

journal homepage: www.elsevier.com/locate/he

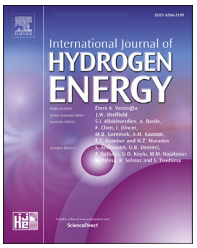

Improvements in hydrogen production from methane dry reforming on filament-shaped mesoporous alumina-supported cobalt nanocatalyst

Ngoc Thang Tran [a,b], *Thong Le Minh Pham* [c], *Trinh Duy Nguyen* [d], *Nguyen Van Cuong* [b], *Tan Ji Siang* [a], *Pham T.T. Phuong* [e], *A.A. Jalil* [f], *Quang Duc Truong* [g], *Sumaiya Zainal Abidin* [a], *Ftwi Y. Hagos* [h], *Sonil Nanda* [i], *Dai-Viet N. Vo* [d,*]

[a] *Faculty of Chemical & Natural Resources Engineering, Universiti Malaysia Pahang, Lebuhraya Tun Razak, Gambang, Kuantan, Pahang, 26300, Malaysia*

[b] *Faculty of Chemical Engineering, Industrial University of Ho Chi Minh City, 12 Nguyen Van Bao St, Go Vap, Ho Chi Minh City, 7000, Viet Nam*

[c] *Institute of Research and Development, Duy Tan University, Da Nang City, 550000, Viet Nam*

[d] *Center of Excellence for Green Energy and Environmental Nanomaterials (CE@GrEEN), Nguyen Tat Thanh University, 300A Nguyen Tat Thanh, District 4, Ho Chi Minh City, 755414, Viet Nam*

[e] *Institute of Chemical Technology, Vietnam Academy of Science and Technology, 1 Mac Dinh Chi Str., Dist.1, Ho Chi Minh City, Viet Nam*

[f] *School of Chemical and Energy Engineering, Faculty of Engineering, Universiti Teknologi Malaysia, UTM Johor Bahru, 81310, Johor, Malaysia*

[g] *Institute of Multidisciplinary Research for Advanced Materials, Tohoku University, Katahira 2-1-1, Aoba-Ku, Sendai, 980-8577, Japan*

[h] *Automotive Engineering Centre, Universiti Malaysia Pahang, Pekan, Pahang, 26600, Malaysia*

[i] *Department of Chemical and Biochemical Engineering, University of Western Ontario, London, ON, Canada*

HIGHLIGHTS

- Filament-shaped Al_2O_3 was synthesized by evaporation-induced self-assembly method.
- 10%Co/Al_2O_3 exhibited a comparable activity to noble catalysts.
- H_2/CO ratio from methane dry reforming was obtained from 0.6 to 0.9.

GRAPHICAL ABSTRACT

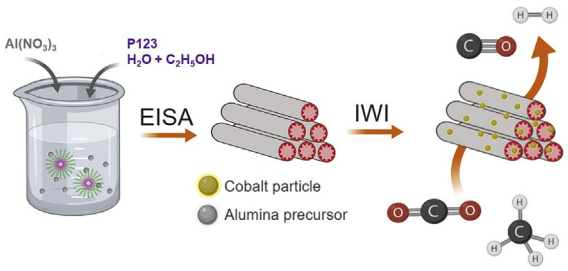

* *Corresponding author.*
E-mail addresses: vndviet@ntt.edu.vn, daivietvnn@yahoo.com, vo.nguyen.dai.viet@gmail.com (D.-V.N. Vo).

https://doi.org/10.1016/j.ijhydene.2020.06.142

ARTICLE INFO

Article history:
Received 6 September 2019
Received in revised form
25 May 2020
Accepted 15 June 2020
Available online xxx

Keywords:
Mesoporous alumina
Cobalt catalyst
Hydrogen
Syngas
Methane dry reforming

ABSTRACT

The mesoporous gamma-alumina (γ-Al_2O_3) synthesized via evaporation-induced self-assembly method (EISA) using inorganic salt, $Al(NO_3)_3 \cdot 9H_2O$ precursor and water-ethanol solvent mixture was implemented as a support for Co catalyst in methane dry reforming at 973–1073 K under 1 atm. The γ-Al_2O_3 support possessed filament-shaped morphology with surface area of 173.4 $m^2\ g^{-1}$ and cobalt nanoparticles were successfully dispersed on support with small crystallite size of 7.8 nm. The stability of 10%Co/Al_2O_3 was evident for CH_4 and CO_2 conversions at 1023 and 1073 K. CH_4 conversion could reach to 76.2% while 81.6% was observed for CO_2 conversion at 1073 K. Although graphitic and amorphous carbons were unavoidably formed on used catalyst, 10%Co/Al_2O_3 exhibited an outstanding performance comparable to noble metals with the desired ratio of H_2/CO for downstream Fischer-Tropsch process.

Introduction

The supplies of energy resources such as petroleum-based fuels are generally recognized to be finite and going to be depleted in next century. Meanwhile, the increase in the average atmospheric temperature and climate change due to greenhouse gases (GHGs) effect mainly induced by anthropogenic CO_2 emissions from fossil fuels combustion are currently presenting serious global issues. For addressing these imperative issues, the replacement of petroleum-derived fuels by alternative and renewable energies is one of the potential approaches. Amongst sustainable fuels, syngas containing CO and H_2 is considered as an emerging and green energy source. Methane dry reforming (MDR as given in Eq. (1)) has emerged as a promising multipurpose pathway for converting two major greenhouse gasses, *viz.*, carbon dioxide (CO_2) and methane (CH_4) to syngas, which is a worthy feedstock for green petrochemicals production [1–6]. Although this method can provide several environmental and economic incentives, the drawbacks relating to its catalytic usage such as expensiveness and/or low operational stability have impeded its large-scale applications. It is well known that noble metals, i.e., Rh and Ru can exhibit high catalytic performance for MDR reaction in terms of the reactant conversions and coking resistance [7].

$$CH_4 + CO_2 \rightarrow 2CO + 2H_2 \quad (1)$$

However, their limited availability and expensiveness are the core obstacles to hinder these catalysts from extensive commercialization. Cobalt- and nickel-based catalysts have recently received significant attentions from an economical viewpoint since they are low-cost and own a comparable catalytic activity to precious metals [8,9]. Nevertheless, the implementation of Ni-containing catalysts could induce carbonaceous deposition on catalyst surface and catalyst bed resulting in catalytic deactivation and reactor blockage, respectively [9,10]. Cobalt has proved itself as a potential catalyst in industrial scale applications because of its superior thermal stability during reforming reactions [9]. The degree of carbon formation on cobalt-based catalysts mainly originates from methane disproportion on catalyst surface [11]. In fact, carbon formation was reportedly associated with metal particle size larger than 10 nm [12–14]. Therefore, high surface area bearing materials have widely been employed as support for facilitating metal dispersion and active nanoparticles confinement inside the pore channels to prevent metals from welding through the reaction [11,15–17].

Mesoporous alumina has appeared to be a promising carrier material due to its abundant availability and great stability against temperature changes. Essentially, the controllable pore size of alumina material by adjusting synthesis parameters is a key factor for manipulating support with a desired structure [18,19]. In general, the conventional evaporation-induced self-assembly (EISA) method for mesoporous alumina preparation normally employs structure-directing polymer template, aluminum alkoxides and anhydrous alcohol solvent [18,20]. However, from the economic and environmental perspectives, the organic aluminum precursors used in EISA approach for mesoporous Al_2O_3 synthesis are quite expensive and harmful to the environment [21]. Thus, implementing less expensive and highly available inorganic aluminum precursor is gaining an alluring interest. The combination of cobalt active metal and mesoporous Al_2O_3 produced by EISA method has not been fully explored for MDR before. Hence, the goals of this research are to synthesize the mesoporous Al_2O_3 support by EISA method using an aluminum nitrate nonahydrate precursor and evaluate the catalytic performance of cobalt supported on as-prepared Al_2O_3 for MDR at varied temperatures.

Experimental section

Materials

Aluminum nitrate nonahydrate ($Al(NO_3)_3 \cdot 9H_2O$) and hydrochloric acid (HCl, 37%) were obtained from Merck Millipore while tri-block-poly (ethylene glycol)-block-poly (propylene glycol)-block-poly (ethylene glycol), Pluronic® P-123 ($EO_{20}PO_{70}EO_{20}$) and $Co(NO_3)_2 \cdot 6H_2O$ (98% purity) were procured from Sigma-

Please cite this article as: Tran NT et al., Improvements in hydrogen production from methane dry reforming on filament-shaped mesoporous alumina-supported cobalt nanocatalyst, International Journal of Hydrogen Energy, https://doi.org/10.1016/j.ijhydene.2020.06.142

Aldrich, St. Louis, Missouri, USA. Ethanol (99.9% purity) was supplied by VWR Chemicals, Heverlee, Belgium. All the chemicals employed in this study were procured from above-mentioned suppliers and used directly without any purification.

Catalyst preparation

In order to synthesize the mesoporous γ-alumina support, about 1.96 g of Pluronic® P-123 template was dissolved in 29.5 mL of a mixed solvent (containing 25% water and 75% ethanol by volume) in a paraffin-covered Pyrex beaker. This mixture was magnetically stirred for 30 min at ambient temperature followed by pouring 7.36 g of $Al(NO_3)_3 \cdot 9H_2O$ powder. About 3.14 mL of HCl (37%) was subsequently added dropwise to the aforementioned solution. The resulting mixture was thoroughly stirred for 1 h before the 24 h of hydrothermal treatment in a Teflon-covered corrosion-resistant autoclave at 373 K. The cooled mixture was slowly dispensed into a beaker and subsequently dried in a Memmert UF1060 oven (Schwabach, Germany) for 48 h at 333 K. The obtained sticky gel was further calcined at 1073 K in a muffle furnace (Carbolite CWF 1200, Sheffield, UK) over 5 h to form mesoporous alumina. After calcination, the resulting Al_2O_3 support was sieved to uniform particle size within 125–160 μm for further catalyst synthesis.

Supported cobalt was prepared via an incipient wetness impregnation (IWI) technique. About 0.568 g of metal precursor, $Co(NO_3)_2 \cdot 6H_2O$, previously dissolved in 0.5 mL of anhydrous C_2H5OH was dropped on 1 g of as-prepared alumina support and mixed in the rotary evaporator (BÜCHI Rotavapor R-200) for 1 h under vacuum condition. Overnight drying at 373 K and 5 h of static air calcination at 873 K with 1 K min^{-1} ramping rate for freshly impregnated mixture were conducted to produce 10%Co/Al_2O_3. The detailed schematic diagram for Al_2O_3 and 10%Co/Al_2O_3 synthesis procedure is also given in Fig. S1 (see supplementary data) to illustrate the aforementioned preparation steps.

Catalyst characterization

The N_2 adsorption/desorption behaviors of Al_2O_3 and 10%Co/Al_2O_3 were analyzed using an automated Tristar II 3020 (Micromeritics, Norcross, GA, USA) gas adsorption device using liquid N_2 at 77 K. Each sample was degassed for 1 h by the flow of hot nitrogen at 573 K before measurement. The phases and crystalline structures were identified by the bench-top Rigaku Miniflex 600 (Rigaku, Tokyo, Japan) X-ray analyzer (XRD) employing a copper radiation source (Cu Kα, λ = 1.5418 Å). Diffraction scanning at 3-80° with a scan rate of 1°min^{-1} and a step of 0.02° was set for all samples.

The reduction behavior of active phases in the catalyst was examined through temperature-programmed reduction (H_2-TPR) using the AutoChem II-2920 unit (Micromeritics, Georgia, USA). About 50 mg of catalyst was sandwiched and positioned at center of U-tube (quartz material). Subsequently, this sample was undergone pretreatment to eradicate moisture and volatile compounds under N_2 gas at 373 K for 0.5 h followed by reduction with 50 mL min^{-1} of 10%H_2/N_2. The temperature was raised to 1173 K at a speed of 10 K min^{-1} and hold for 30 min at a constant temperature of 1173 K before being cooled down in N_2 atmosphere.

The extent of carbon deposition on the catalyst after MDR was quantified based on the weight loss during temperature-programmed oxidation (TPO). The TGA Q500 analyzer (TA Instruments, Newcastle, DE, USA) was employed for TPO runs. Dehydration under 100 mL min^{-1} of N_2 gas at 373 K for 0.5 h was initially conducted to eliminate moisture content. The process continued with specimen oxidation by alternating the N_2 medium to mixed gases of 20 mL min^{-1} O_2 and 80 mL min^{-1} N_2 and subsequently raising the temperature to 1023 K with 10 K min^{-1} followed by holding for 30 min at 1023 K.

Raman scattering spectrum was obtained using a NRS-3100 Raman spectrometer (JASCO, Tokyo, Japan) equipped with a 532 nm laser wavelength. The spectroscopic measurements were conducted in ambient air. The morphology of catalyst was examined via a high-resolution transmission electron microscopy (HRTEM) conducted in a TOPCOM EM-002B microscope.

Catalytic activity evaluation

A fixed-bed reactor (length: 17 in. and diameter: 3/8 in.) was employed for testing the 10%Co/Al_2O_3 for MDR (see Fig. S2 in supplementary data). Roughly 0.1 g of catalyst was located at the middle of reactor by quartz wool whilst gaseous reactants and inert N_2 gas were exactly controlled by Alicat mass flow controllers and mixed before entering the MDR reactor. The MDR reaction was carried out with gas hourly space velocity (GHSV) of 36 L g_{cat}^{-1} h^{-1} at temperature range from 973 K to 1073 K and stoichiometric feed ratio. The selection of high GHSV, small catalyst loading and tiny particle size is to assure the negligible presence of mass and heat transfer resistances and hence obtaining the intrinsic catalytic activity. The detailed calculation for avoiding these mass and heat transfer intrusions is given in the supplementary data. Prior to the assessment, in-situ H_2 reduction was executed for 1 h at 1073 K with a gas mixture of 50%H_2/N_2 (60 mL min^{-1}) to activate catalyst bed. All gaseous products and unreacted reactants were analyzed using an Agilent 6890 Gas Chromatography (Santa Clara, California, USA) equipped with a HP-PLOT Q capillary column and a TCD detector.

The conversion of reactants (X_i with i: CH_4 or CO_2), product yields (Y_{CO}[fx] and Y_{H_2}) and H_2/CO ratio were calculated using these corresponding Eqs. (2)–(5) based on the inlet, F^{in} and outlet, F^{out} flow rates (mol s^{-1}).

$$X_i(\%) = \frac{F_i^{in} + F_i^{out}}{F_i^{in}} \times 100\% \quad (2)$$

$$Y_{CO}(\%) = \frac{F_{CO}^{out}}{F_{CH_4}^{in} + F_{CO_2}^{in}} \times 100\% \quad (3)$$

$$Y_{H_2}(\%) = \frac{F_{H_2}^{out}}{2F_{CH_4}^{in}} \times 100\% \quad (4)$$

$$\frac{H_2}{CO} = \frac{F_{H_2}^{out}}{F_{CO}^{out}} \quad (5)$$

The carbon material balance was conducted for each run with time-on-stream and the error of it was within 1.8–3.7%. In addition to carbon mass balance, N_2 internal standard was

Please cite this article as: Tran NT et al., Improvements in hydrogen production from methane dry reforming on filament-shaped mesoporous alumina-supported cobalt nanocatalyst, International Journal of Hydrogen Energy, https://doi.org/10.1016/j.ijhydene.2020.06.142

used during MDR to justify the accuracy of GC analytical analysis and the small discrepancy was less than 5.18%. In order to verify the active role of Co metal in MDR, the blank MDR experiment on bare Al_2O_3 support at stoichiometric feed composition and 1023 K was also carried out. As seen in Fig. S3 (supplementary data), Al_2O_3 was actually not inert but slightly catalyzed methane cracking due to high reaction temperature. Nevertheless, the conversion of CH_4 and CO_2 was substantially low (about 1.6% and 6.0%, respectively) on Al_2O_3. This would indicate that the higher conversion values than abovementioned extents belong to the function of Co active metal.

Results and discussion

Characterization of fresh materials

Textural attributes

The N_2 adsorption-desorption isotherms of γ-Al_2O_3, fresh and spent 10%Co/Al_2O_3 are depicted in Fig. 1. The isotherm curves of both support and fresh catalyst were classified as type IV and had H1 hysteresis loops based on IUPAC category indicating that the mesoporous support and catalyst possessed cylindrical pore geometry [22]. In addition, the steep condensation stage for both samples signifies the relatively high pore size uniformity and confirms the presence of wide mesopores [23]. As seen in Fig. 1, the isotherm curves of fresh 10%Co/Al_2O_3 show an analogous shape to those of γ-Al_2O_3 support suggesting that the structural feature of γ-Al_2O_3 was maintained during inserting Co_3O_4 particles into its cavities. Notably, the isotherm shape of spent catalysts collected from various MDR reaction temperature from 973 to 1073 K was also unchanged. This could suggest that the textural structure of catalyst was stable with reaction temperature.

Additionally, the pore size distribution (PSD) of both materials computed by Barret–Joyner–Halenda (BJH) method using desorption branch is shown in Fig. 2. The narrow diameter range of 2–12 nm with the main pore size of 6 nm

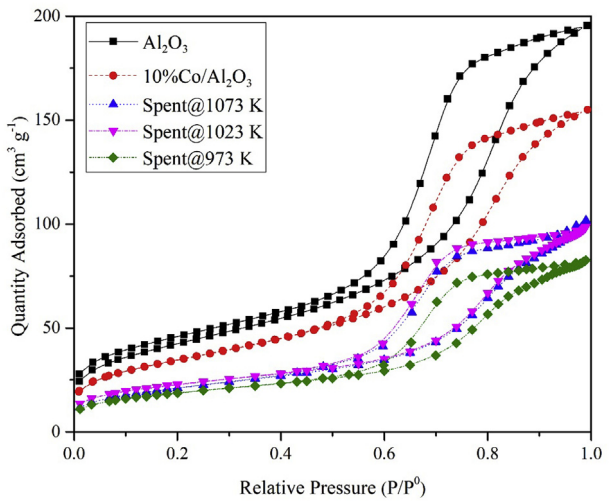

Fig. 1 – N_2 physisorption plots of Al_2O_3, fresh 10%Co/Al_2O_3 and spent catalysts at different reaction temperature.

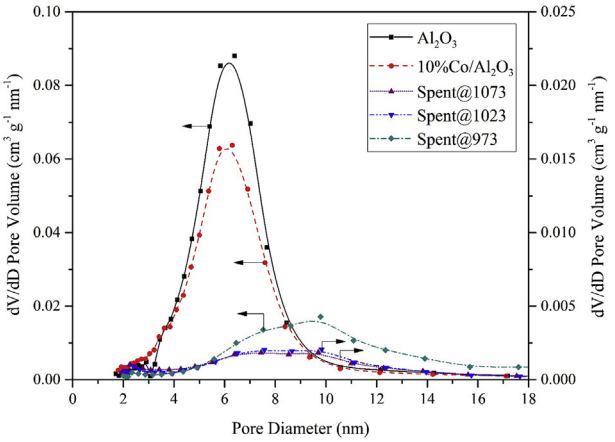

Fig. 2 – Pore size distribution plots for Al_2O_3, fresh 10%Co/Al_2O_3 and spent catalysts at different reaction temperature.

was evidenced for both support and fresh catalyst further confirming the structure preservation of γ-Al_2O_3 support [24]. Thus, the peak shift for spent catalysts to 8–10 nm (see Fig. 2) could be attributed to the presence of deposited carbon on catalyst surface after reaction.

Table 1 summarizes the detailed textural features of γ-Al_2O_3, fresh and spent 10%Co/Al_2O_3. The BET surface area of γ-Al_2O_3 about 173.4 $m^2\ g^{-1}$ was slightly higher than that of fresh 10%Co/Al_2O_3 (141.9 $m^2\ g^{-1}$). The minor drop in BET surface area of catalyst was reasonably owing to the unchanged structure of γ-Al_2O_3 support during IWI procedure. The total pore volume (0.28 $cm^3\ g^{-1}$) and mean pore diameter (6.48 nm) of support also dropped with the introduction of Co metal oxides. This would be an indicative of successful diffusion of Co oxide particles into the porous structure of γ-Al_2O_3 support. The drop in BET surface area of spent catalysts ranging from 66 to 79 $m^2\ g^{-1}$ was not avoidable because of carbon formation blocking the porous support structure.

XRD measurements

X-ray diffractograms of Al_2O_3, calcined and reduced 10%Co/Al_2O_3 are displayed in Fig. 3. The Joint Committee on Powder

Table 1 – Summary of textural attributes of γ-Al_2O_3 and 10%Co/Al_2O_3.

Samples	BET surface area ($m^2\ g^{-1}$)	Total pore volume ($cm^3\ g^{-1}$)	Average pore diameter (nm)	Mean Co_3O_4 crystallite size (nm)[a]
γ-Al_2O_3	173.4	0.28	6.48	–
Fresh 10%Co/Al_2O_3	141.9	0.22	6.28	7.8
Spent@1073 K	75.0	0.16	7.97	–
Spent@1023 K	79.0	0.16	8.00	–
Spent@973 K	65.7	0.13	7.83	–

[a] Calculated using Scherrer equation [25] for Co_3O_4 peak at $2\theta = 31.32°$.

Please cite this article as: Tran NT et al., Improvements in hydrogen production from methane dry reforming on filament-shaped mesoporous alumina-supported cobalt nanocatalyst, International Journal of Hydrogen Energy, https://doi.org/10.1016/j.ijhydene.2020.06.142

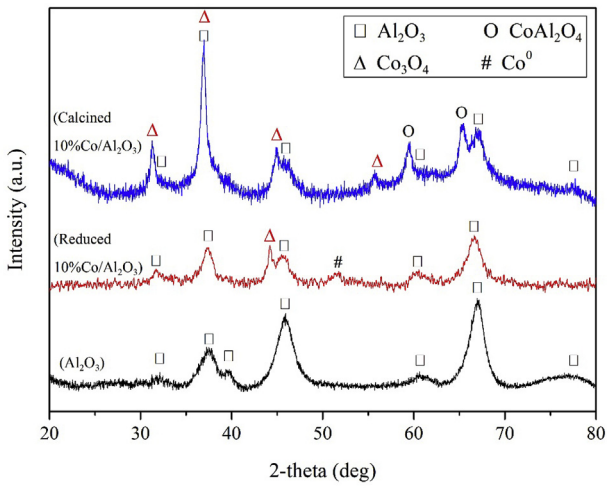

Fig. 3 – XRD spectra of Al_2O_3, calcined and reduced 10%Co/Al_2O_3.

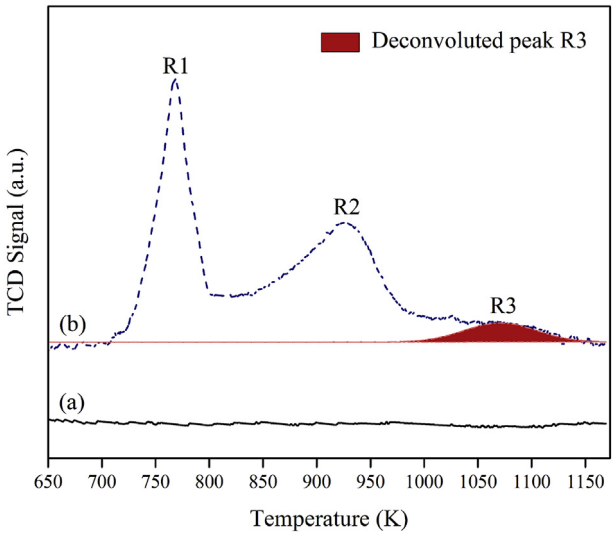

Fig. 4 – H_2-TPR profiles of (a) Al_2O_3 and (b) 10%Co/Al_2O_3.

Diffraction Standards (JCPDS) was employed as the references to identify diffraction peaks for all samples [26]. The peaks at 2θ of 32.05°, 37.40°, 39.58°, 45.96°, 60.76°, 67.02° and 77.11° were assigned to γ-Al_2O_3 planes while the peaks detected at 2θ of 31.32°, 37.03°, 44.88° and 55.82° indicated the presence of Co_3O_4 phase (JCPDS card No. 74–2120). The strong interaction of CoO and Al_2O_3 phases was also confirmed by the presence of distinct peaks at 59.62° and 65.42° that belong to cobalt-aluminate spinel, $CoAl_2O_4$ (JCPDS card No. 82–2246).

For the reduced catalyst, the peak of Co^0 metallic phase appeared at 2θ of 51.50° (JCPDS card No. 15–0806) and there is no signal of $CoAl_2O_4$ phase indicating the effective and complete $CoAl_2O_4$ reduction to Co^0 particles. Nevertheless, the Co^0 phase could be partially oxidized to Co_3O_4 when it was exposed to oxygen in air during XRD measurement as evidenced by the small intensity peak at 2θ of 44.88°.

The mean crystallite size of Co_3O_4 calculated using Scherrer equation (Eq. (6)) is about 7.8 nm. The smaller Co_3O_4 crystallite size than 10 nm was reportedly preferred due to the higher portion of corner and edge surface sites as well as lower possibility for coke formation requiring large terrace atoms for nucleation [27].

$$d_{Co_3O_4} = \frac{0.94 \times \lambda}{\beta \times Cos\theta} \quad (6)$$

where λ is the radiation wavelength and β stands for the full-width at half-maximum (FWHM) of calculated peak at 2θ Bragg angle.

Reducibility study

The reducibility of catalyst is verified via H_2-TPR measurement as shown in Fig. 4. Fig. 4(a) displays the reducing profile of Al_2O_3 and there is no noticeable peak for Al_2O_3 reduction indicating a stable support during catalytic activation in H_2. The H_2-TPR profile of 10%Co/Al_2O_3 (Fig. 4(b)) shows the appearance of three distinct peaks labelled as R1, R2 and R3 located at 768 K, 913 K and 1084 K, respectively. The assignments of the detected peaks are summarized in Table 2. The first peak R1 was ascribed for Co_3O_4 reduction to CoO intermediary whilst the peak R2 represented the transformation of Co (II) oxide into Co^0 metallic form [28,29]. The reduction of $CoAl_2O_4$ spinel phase was also evidenced by peak R3. The lowest intensity of peak R3 compared to peaks R1 and R2 could indicate that the amount of $CoAl_2O_4$ spinel form was significantly lower than that of Co_3O_4. Thus, the presence of lesser $CoAl_2O_4$ amount compared with the preferred Co_3O_4 phase would not substantially affect the catalytic performance.

Table 2 – Summary of peak assignment during H_2 reduction of 10%Co/Al_2O_3.

Peak	Temperature (K)	Peak Assignment
R1	768	$Co_3O_4 + H_2 \rightarrow 3CoO + H_2O$
R2	913	$CoO + H_2 \rightarrow Co + H_2O$
R3	1084	$CoAl_2O_4 + H_2 \rightarrow Co^0 + Al_2O_3 + H_2O$

Surface morphology analyses

The HRTEM images of fresh γ-Al_2O_3 and 10%Co/Al_2O_3 is shown in Fig. 5. The γ-Al_2O_3 support has a filamentous shape with various sizes (see Fig. 5(a)). Interestingly, the filament-shaped Al_2O_3 was also spotted in 10%Co/Al_2O_3 as displayed in Fig. 5(b). This observation further corroborates the unchanged structure of support in calcination during catalyst synthesis. Additionally, the filamentous configuration of alumina with defined diameters approximately less than 10 nm was observed in both HRTEM patterns and cobalt oxide nano-grains seem to be well dispersed onto the porous γ-Al_2O_3.

Catalytic performance for MDR

The performance of 10%Co/Al_2O_3 catalyst was evaluated at varied temperatures of 973, 1023 and 1073 K while keeping the feed ratio at the stoichiometric condition. The influence of temperature on conversion of CH_4 and CO_2 with time-on-stream (TOS) is depicted in Figs. 6 and 7, respectively. Both reactant conversions enhanced greatly with rising

Please cite this article as: Tran NT et al., Improvements in hydrogen production from methane dry reforming on filament-shaped mesoporous alumina-supported cobalt nanocatalyst, International Journal of Hydrogen Energy, https://doi.org/10.1016/j.ijhydene.2020.06.142

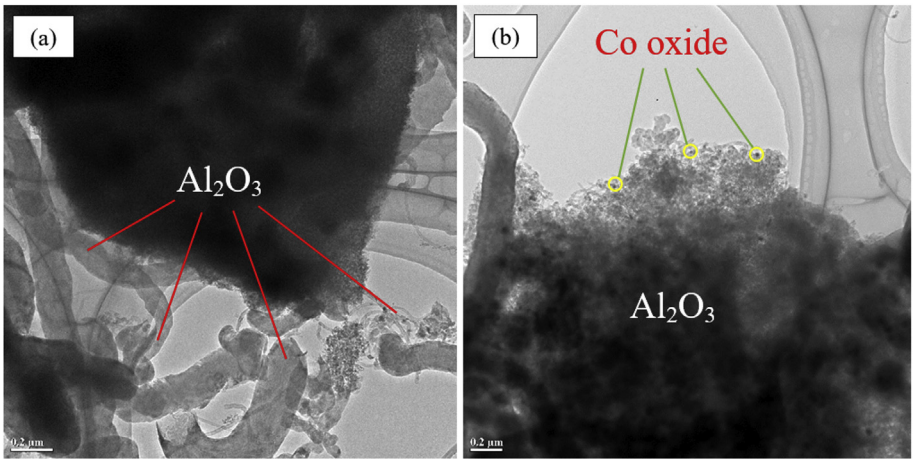

Fig. 5 – HRTEM images of fresh (a) Al_2O_3 and (b) 10%Co/Al_2O_3.

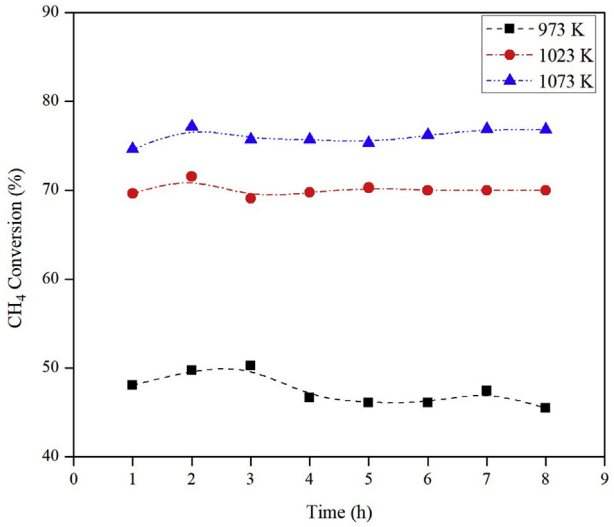

Fig. 6 – CH_4 conversion with TOS on 10%Co/Al_2O_3 at stoichiometric feed composition and temperature of 973–1073 K.

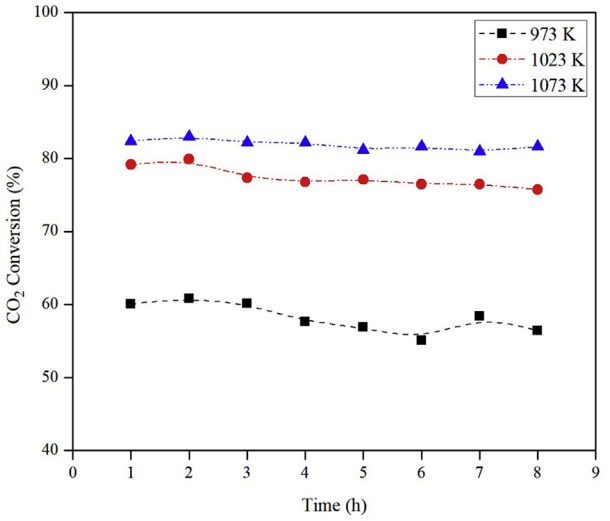

Fig. 7 – CO_2 conversion with TOS on 10%Co/Al_2O_3 at stoichiometric feed composition and temperature of 973–1073 K.

temperature from 973 to 1073 K. In particular, CH_4 conversion increased from ca. 46.1%–76.2% while an increase from around 55.1%–81.6% was evidenced for CO_2 conversion. These observations are reasonably due to the endothermic nature of MDR favored at high temperature [6]. As seen in Figs. 6 and 7, the conversion of CH_4 and CO_2 seemed to be unchanged with TOS at 1023 K and 1073 K. However, reactant conversions exhibited a decline with time at low temperature of 973 K. This unstable activity could be attributed to the oxidation of Co^0 metallic phase to an inactive form by excessive oxygen species from dissociative CO_2 adsorption [9,10].

The influence of temperature on the yield for CO and H_2 as well as H_2/CO ratio is illustrated in Fig. 8. Both H_2 and CO yields elevated extensively with an increase in the reforming temperature. Particularly, the yield of H_2 enhanced from 27.5% at 973 K to 63.6% at 1073 K whereas a rise from 43.9% to 68.9% was observed for CO yield with increasing temperature from 973 to 1073 K. As seen in Fig. 8, for all temperatures, the H_2/CO proportions were consistently lower than the stoichiometric proportion of one (cf. Eq. (1)). This could be assigned to the parallel presence of reverse water-gas shift side reaction (RWGS, Eq. (7)) concurrently consuming H_2 and producing extra CO gas [30,31].

$$CO_2 + H_2 \rightleftarrows CO + H_2O \quad (7)$$

Apart from RWGS, the H_2/CO ratio is also interfered by other side reactions, *viz.*, CH_4 decomposition and reverse Boudouard reactions. As shown in Fig. 8, the increase in H_2/CO ratio with growing reaction temperature from 973 to 1073 K could be indicative of dominant CH_4 decomposition contributing to rising H_2 formation. Nevertheless, the low values of H_2/CO ratio from 0.6 to 0.9 seem to be within preferred range used for long-chain hydrocarbon production in Fischer-Tropsch synthesis [32–34].

For assessing the efficacy of mesoporous filament-shaped γ-Al_2O_3 supported Co catalyst for MDR, commercial γ-Al_2O_3-supported Co and other catalysts recently used in the MDR

Please cite this article as: Tran NT et al., Improvements in hydrogen production from methane dry reforming on filament-shaped mesoporous alumina-supported cobalt nanocatalyst, International Journal of Hydrogen Energy, https://doi.org/10.1016/j.ijhydene.2020.06.142

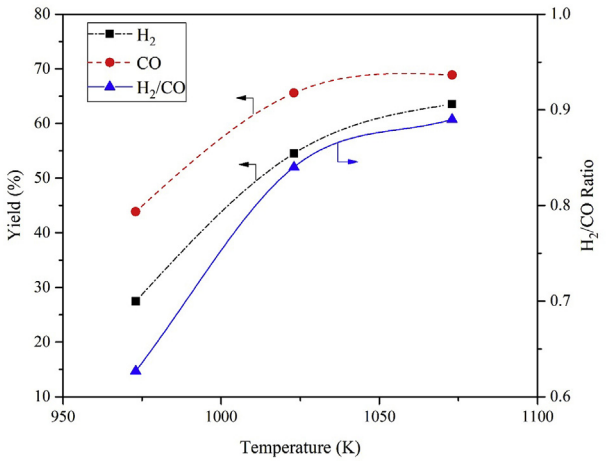

Fig. 8 – Influence of reaction temperature on gaseous product yields and H_2/CO ratio for 10%Co/Al_2O_3 at stoichiometric feed ratio.

reaction are summarized in Table 3. In particular, the superior role of mesoporous filament-shaped γ-Al_2O_3 support is justified through the comparison with commercial γ-Al_2O_3 support (denoted as γ-Al_2O_3®, Puralox SCCa-150/200) from Sasol. As seen in Table 3, 10%Co/Al_2O_3®, prepared using the same IWI technique as the mesoporous 10%Co/Al_2O_3 in this study, exhibited a lower CH_4 conversion of 56.3% than this of mesoporous 10%Co/Al_2O_3 (70%) at similar MDR conditions. In comparison with other Co-based catalysts in literature, our catalyst exhibited higher or relatively comparable CH_4 conversion although MDR runs were conducted at a greater GHSV = 36 L g_{cat}^{-1} h^{-1} in this work. Although the activity of our catalyst is slightly lower than noble metal catalysts such as 5% Ru/Al_2O_3 [35] and 0.5%Pd6%Ni/Al_2O_3 [16], from the industrial and economical points of view, the 10%Co/Al_2O_3 catalyst in this study could be a potential catalyst for large-scale production of syngas through MDR.

Spent catalysts characterization

TPO measurements

The amounts of deposited carbon on the spent 10%Co/Al_2O_3 after MDR at 973, 1023 and 1073 K are demonstrated via sample weight loss in thermal oxidation analysis as shown in Fig. 9. The weight drop in all TPO curves observed at temperature greater than 700 K was attributed to the oxidation of amorphous and graphitic carbons deposited on catalyst surface [42]. The accumulated carbon after 8 h of reactions at 973, 1023 and 1073 K was 27.9%, 47.7% and 38.6%, respectively. Carbon deposition in MDR is unavoidable and primarily depends on the extent of endothermic methane disproportion (see Eq. (8)) [43]. Thus, the lowest amount of deposited carbon of 27.9% was observed at 973 K and it increased to 47.7% with rising temperature from 973 K to 1023 K. Nevertheless, a considerable decline in carbonaceous formation from 47.7% to 38.6% at 1073 K was credited to the presence of reverse Boudouard reaction (cf. Eq. (9)).

$$CH_4 \rightarrow C + 2H_2 \quad (8)$$

$$C + CO_2 \rightleftarrows 2CO \quad (9)$$

Additionally, as seen in Fig. 9, the derivative weight profiles of all three spent catalysts disclosed two kinds of deposited carbon evidenced via the detection of peaks A and B. The first peaks (A) appearing at temperature lower than 850 K corresponded to the oxidation of active amorphous carbon while the second peaks (B) were assigned to the less-reactive graphitic carbon requiring greater oxidation temperature to be removed from catalyst surface [42].

Raman spectroscopy

To verify the type of carbon deposition, selected used catalyst was subject to Raman measurement. Fig. 10 shows the Raman spectra of support as well as fresh and used 10%Co/Al_2O_3 collected from MDR for 8 h at 1023 K. For the fresh catalyst (Fig. 10(a)), four peaks at 473.9, 517.7, 609.7 and 678.5 cm^{-1}

Table 3 – Summary of MDR performance over different catalysts reported in literature.

Catalyst	Reaction conditions			CH_4 conversion (%)	H_2:CO ratio	Refs.
	T (K)	GHSV (L g_{cat}^{-1} h^{-1})	TOS (h)			
5%Ru/Al_2O_3	1073	60	0.5	84.4	n.m.[a]	[35]
0.5%Pd6%Ni/Al_2O_3	1023	24	n.m.	86.0	n.m.	[16]
10%Ni/ZrO_2	1023	24	10	60.0	n.m	[36]
7%Ni/ZSM-5	1073	60	12	66.3	n.m.	[37]
10%Ni/SBA-15	1073	36	8	62.0	n.m.	[38]
10%Co/SBA-15	973	1.2	5	23.9	0.34	[15]
20%Co/La_2O_3	1023	15	n.m.	49.1	n.m.	[39]
20%Co/CeO_2	1023	15	4	71.5	1.30	[30]
10%Co/Y Zeolite	1123	24	10	79.7	0.78	[40]
20%Co/Nd_2O_3	1023	15	n.m.	63.5	n.m.	[41]
10%Co/Al_2O_3	973	36	8	47.5	0.63	This study
	1023	36	8	70.0	0.84	This study
	1073	36	8	76.2	0.89	This study
10%Co/Al_2O_3® (Commercial support)[b]	1023	36	8	56.3	0.83	This study

[a] n.m.: not mentioned.
[b] Calcined γ-Al_2O_3 support (Puralox SCCa-150/200) obtained from Sasol.

Please cite this article as: Tran NT et al., Improvements in hydrogen production from methane dry reforming on filament-shaped mesoporous alumina-supported cobalt nanocatalyst, International Journal of Hydrogen Energy, https://doi.org/10.1016/j.ijhydene.2020.06.142

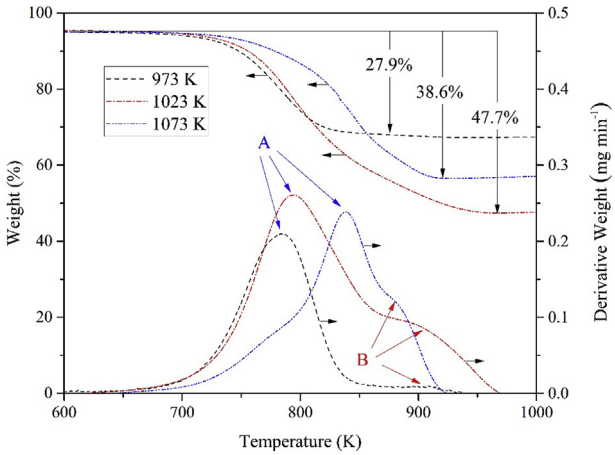

Fig. 9 – TPO weight and derivative weight profiles of spent Co/Al_2O_3 after MDR reactions at 973 K, 1023 K, and 1073 K.

correspond to the Raman vibrational modes of E_g (473.9 cm^{-1}), F_{2g} (517.7 and 609.7 cm^{-1}) and A_{1g} (678.5 cm^{-1}). These characteristic peaks were attributed to Co_3O_4 crystalline form [42,44] in agreement with XRD patterns (see Fig. 3). As seen in Raman spectrum of used sample (Fig. 10(b)), the appearance of two intense peaks so-called D-band and G-band at 1338.5 cm^{-1} and 1573.5 cm^{-1}, respectively evidenced the co-presence of amorphous and ordered graphitic carbons on used catalyst surface in agreement with TPO results (see Fig. 9) [42,45]. In fact, D-band was attributed to the disorder in sp^3-hybridized carbon systems for amorphous carbon or carbon nanofibers while the G-band resulted from the C=C bond stretching in the high-order graphitic materials [45]. The inset in Fig. 10 belonging to the Raman spectra of Al_2O_3 shows 5 main peaks at 377.5, 418.0, 576.7, 643.0 and 750.1 cm^{-1} which are typical peaks of Al_2O_3 support [46,47]. The absence of these peaks in both fresh and spent catalysts was due to the thorough surface Al_2O_3 coverage by Co_3O_4 particles [47].

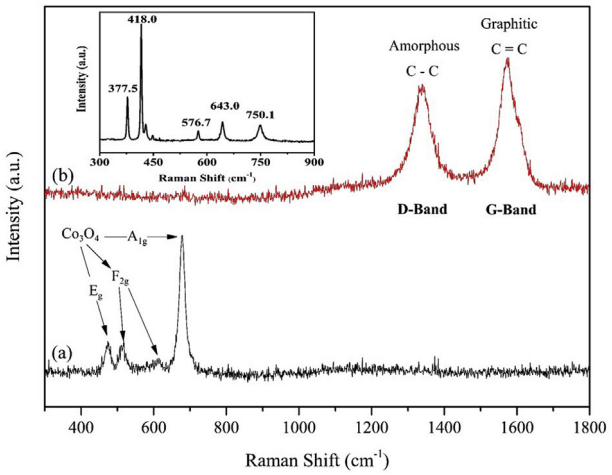

Fig. 10 – Raman spectra for (a) fresh $10\%Co/Al_2O_3$ and (b) used $10\%Co/Al_2O_3$ after MDR at 1023 K with stoichiometric reactant composition.

Conclusions

The filament-shaped mesoporous alumina-supported cobalt catalyst successfully synthesized through the EISA and IWI approaches was evaluated for MDR at different temperatures of 973–1073 K Co_3O_4 nanoparticles were effectively dispersed on mesoporous support and owned a small crystallite size of 7.8 nm Co_3O_4 and $CoAl_2O_4$ phases formed on catalyst surface were reduced to Co^0 metallic form in H_2 activation. The 10% Co/Al_2O_3 demonstrated catalytic stability during 8 h on-stream at 1023 K and 1073 K. Increasing reaction temperature enhanced CH_4 and CO_2 conversions to approach 76.2% and 81.6%, respectively at 1073 K. Additionally, H_2/CO ratio changed from 0.6 to 0.9 depending on reaction temperature and the low value of it was suitable for high molecular weight hydrocarbon production in downstream CO hydrogenation. $10\%Co/Al_2O_3$ exhibited a relatively comparable activity to noble catalysts reported in literature. The presence of graphitic and amorphous carbons was inevitable due to CH_4 decomposition; however, the amount of carbonaceous species was reduced at 1073 K owing to reverse Boudouard side reaction.

Declaration of competing interest

The authors declare that they have no known competing financial interests or personal relationships that could have appeared to influence the work reported in this paper.

Acknowledgments

The authors deeply acknowledge the financial support from IUH Research Grant Scheme (44/HĐ-ĐHCN, Code No: 184HH06) to carry out this work. Dr. Nguyen Huu Huy Phuc is also acknowledged for conducting the Raman measurements of our samples.

Appendix A. Supplementary data

Supplementary data to this article can be found online at https://doi.org/10.1016/j.ijhydene.2020.06.142.

REFERENCES

[1] Usman M, Daud WMAW, Abbas HF. Dry reforming of methane: influence of process parameters: a review. Renew Sustain Energy Rev 2015;45:710–44. https://doi.org/10.1016/j.rser.2015.02.026.
[2] Abdullah B, Ghani NAA, Vo D-VN. Recent advances in dry reforming of methane over Ni-based catalysts. J Clean Prod

2017;162:170–85. https://doi.org/10.1016/j.jclepro.2017.05.176.
[3] Vo D-VN, Nguyen TH, Kennedy EM, Dlugogorski BZ, Adesina AA. Fischer-Tropsch synthesis: effect of promoter type on alumina-supported Mo carbide catalysts. Catal Today 2011;175(1):450–9. https://doi.org/10.1016/j.cattod.2011.04.045.
[4] Inderwildi OR, Jenkins SJ, King DA. Mechanistic studies of hydrocarbon combustion and synthesis on noble metals. Angew Chem Int Ed 2008;47(28):5253–5. https://doi.org/10.1002/anie.200800685.
[5] Kapokova L, Pavlova S, Bunina R, Alikina G, Krieger T, Ishchenko A, Rogov V, Sadykov V. Dry reforming of methane over $LnFe_{0.7}Ni_{0.3}O_3$-δ perovskites: influence of Ln nature. Catal Today 2011;164(1):227–33. https://doi.org/10.1016/j.cattod.2010.10.086.
[6] Aramouni NAK, Touma JG, Tarboush BA, Zeaiter J, Ahmad MN. Catalyst design for dry reforming of methane: analysis review. Renew Sustain Energy Rev 2018;82:2570–85. https://doi.org/10.1016/j.rser.2017.09.076.
[7] Pakhare D, Spivey J. A review of dry (CO_2) reforming of methane over noble metal catalysts. Chem Soc Rev 2014;43(22):7813–37. https://doi.org/10.1039/C3CS60395D.
[8] Ruckenstein E, Wang HY. Carbon dioxide reforming of methane to synthesis gas over supported cobalt catalysts. Appl Catal 2000;204(2):257–63. https://doi.org/10.1016/S0926-860X(00)00674-8.
[9] Budiman AW, Song SH, Chang TS, Shin CH, Choi MJ. Dry reforming of methane over cobalt catalysts: a literature review of catalyst development. Catal Surv Asia 2012;16(4):183–97.
[10] Arora S, Prasad R. An overview on dry reforming of methane: strategies to reduce carbonaceous deactivation of catalysts. RSC Adv 2016;6(110):108668–88. https://doi.org/10.1039/C6RA20450C.
[11] Xin J, Cui H, Cheng Z, Zhou Z. Bimetallic Ni-Co/SBA-15 catalysts prepared by urea co-precipitation for dry reforming of methane. Appl Catal 2018;554:95–104. https://doi.org/10.1016/j.apcata.2018.01.033.
[12] Kim JH, Suh DJ, Park TJ, Kim KL. Effect of metal particle size on coking during CO_2 reforming of CH_4 over Ni-alumina aerogel catalysts. Appl Catal 2000;197(2):191–200. https://doi.org/10.1016/S0926-860X(99)00487-1.
[13] Zhang J, Wang H, Dalai AK. Effects of metal content on activity and stability of Ni-Co bimetallic catalysts for CO_2 reforming of CH_4. Appl Catal 2008;339(2):121–9. https://doi.org/10.1016/j.apcata.2008.01.027.
[14] Juan-Juan J, Roman-Martinez MC, Illan-Gomez MJ. Nickel catalyst activation in the carbon dioxide reforming of methane: effect of pretreatments. Appl Catal 2009;355(1-2):27–32. https://doi.org/10.1016/j.apcata.2008.10.058.
[15] Taherian Z, Yousefpour M, Tajally M, Khoshandam B. Catalytic performance of Samaria-promoted Ni and Co/SBA-15 catalysts for dry reforming of methane. Int J Hydrogen Energy 2017;42(39):24811–22. https://doi.org/10.1016/j.ijhydene.2017.08.080.
[16] Ma Q, Sun J, Gao X, Zhang J, Zhao T, Yoneyama Y, Tsubaki N. Ordered mesoporous alumina-supported bimetallic Pd-Ni catalysts for methane dry reforming reaction. Catal Sci Technol 2016;6(17):6542–50. https://doi.org/10.1039/C6CY00841K.
[17] Singh S, Kumar R, Setiabudi HD, Nanda S, Vo D-VN. Advanced synthesis strategies of mesoporous SBA-15 supported catalysts for catalytic reforming applications: a state-of-the-art review. Appl Catal 2018;559:57–74. https://doi.org/10.1016/j.apcata.2018.04.015.
[18] Wu W, Wan Z, Chen W, Zhu M, Zhang D. Synthesis of mesoporous alumina with tunable structural properties. Microporous Mesoporous Mater 2015;217:12–20. https://doi.org/10.1016/j.micromeso.2015.06.002.
[19] Wu W, Zhu M, Zhang D. The role of solvent preparation in soft template assisted synthesis of mesoporous alumina. Microporous Mesoporous Mater 2018;260:9–16. https://doi.org/10.1016/j.micromeso.2017.10.017.
[20] Yuan Q, Yin AX, Luo C, Sun LD, Zhang YW, Duan WT, Liu HC, Yan CH. Facile synthesis for ordered mesoporous γ-aluminas with high thermal stability. J Am Chem Soc 2008;130(11):3465–72. https://doi.org/10.1021/ja0764308.
[21] Yuan Q, Yin AX, Luo C, Sun LD, Zhang YW, Duan WT, Liu HC, Yan CH. Facile synthesis of ordered mesoporous alumina and alumina-supported metal oxides with tailored adsorption and framework properties. Chem Mater 2011;23(5):1147–57. https://doi.org/10.1021/ja0764308.
[22] Siang TJ, Pham TLM, Cuong NV, Phuong PTT, Phuc NHH, Truong QD, Vo D-VN. Combined steam and CO_2 reforming of methane for syngas production over carbon-resistant boron-promoted Ni/SBA-15 catalysts. Microporous Mesoporous Mater 2018;262:122–32. https://doi.org/10.1016/j.micromeso.2017.11.028.
[23] Wang N, Chu W, Zhang T, Zhao XS. Synthesis, characterization and catalytic performances of Ce-SBA-15 supported nickel catalysts for methane dry reforming to hydrogen and syngas. Int J Hydrogen Energy 2012;37(1):19–30. https://doi.org/10.1016/j.ijhydene.2011.03.138.
[24] Khodakov AY, Griboval-Constant A, Bechara R, Villain F. Pore-size control of cobalt dispersion and reducibility in mesoporous silicas. J Phys Chem B 2001;105(40):9805–11. https://doi.org/10.1021/jp011989u.
[25] Patterson AL. The Scherrer formula for X-ray particle size determination. Phys Rev 1939;56(10):978–82. https://doi.org/10.1103/PhysRev.56.978.
[26] JCPDS powder diffraction file. PA: Swarthmore: International Centre for Diffraction Data; 2000.
[27] Da Silva Alm, Den Breejen JP, Mattos LV, Bitter JH, De Jong KP, Noronha FB. Cobalt particle size effects on catalytic performance for ethanol steam reforming: smaller is better. J Catal 2014;318:67–74. https://doi.org/10.1016/j.jcat.2014.07.020.
[28] Jabbour K, El Hassan N, Casale S, Estephane J, El Zakhem H. Promotional effect of Ru on the activity and stability of Co/SBA-15 catalysts in dry reforming of methane. Int J Hydrogen Energy 2014;39(15):7780–7. https://doi.org/10.1016/j.ijhydene.2014.03.040.
[29] Ogo S, Shimizu T, Nakazawa Y, Mukawa K, Mukai D, Sekine Y. Steam reforming of ethanol over K-promoted Co catalyst. Appl Catal 2015;495:30–8. https://doi.org/10.1016/j.apcata.2015.01.018.
[30] Ayodele BV, Khan MR, Cheng CK. Catalytic performance of ceria-supported cobalt catalyst for CO-rich hydrogen production from dry reforming of methane. Int J Hydrogen Energy 2016;41(1):198–207. https://doi.org/10.1016/j.ijhydene.2015.10.049.
[31] Omoregbe O, Danh HT, Nguyen-Huy C, Setiabudi HD, Abidin SZ, Truong QD, Vo D-VN. Syngas production from methane dry reforming over Ni/SBA-15 catalyst: effect of operating parameters. Int J Hydrogen Energy 2017;42(16):11283–94. https://doi.org/10.1016/j.ijhydene.2017.03.146.
[32] Vo D-VN, Arcotumapathy V, Abdullah B, Adesina AA. Non-linear ASF product distribution over alkaline-earth promoted molybdenum carbide catalysts for hydrocarbon synthesis. Catal Today 2013;214:42–9. https://doi.org/10.1016/j.cattod.2013.02.002.
[33] Vo D-VN, Cooper CG, Nguyen TH, Adesina AA, Bukur DB. Evaluation of alumina-supported Mo carbide produced via

Please cite this article as: Tran NT et al., Improvements in hydrogen production from methane dry reforming on filament-shaped mesoporous alumina-supported cobalt nanocatalyst, International Journal of Hydrogen Energy, https://doi.org/10.1016/j.ijhydene.2020.06.142

propane carburization for the Fischer-Tropsch synthesis. Fuel 2012;93:105–16. https://doi.org/10.1016/j.fuel.2011.10.015.
[34] De Klerk A. Fischer-tropsch refining. 1st ed. Weinheim: John Wiley & Sons; 2012.
[35] Hou Z, Chen P, Fang H, Zheng X, Yashima X. Production of synthesis gas via methane reforming with CO_2 on noble metals and small amount of noble-(Rh-) promoted Ni catalysts. Int J Hydrogen Energy 2006;31(5):555–61. https://doi.org/10.1016/j.ijhydene.2005.06.010.
[36] Zhang X, Zhang Q, Tsubaki N, Tan Y, Han Y. Carbon dioxide reforming of methane over Ni nanoparticles incorporated into mesoporous amorphous ZrO_2 matrix. Fuel 2015;147:243–52. https://doi.org/10.1016/j.fuel.2015.01.076.
[37] Estephane J, Aouad S, Hany S, El Khoury B, Gennequin C, El Zakhem H, El Nakat J, Aboukaïs A, Abi Aad E. CO_2 reforming of methane over Ni-Co/ZSM5 catalysts: aging and carbon deposition study. Int J Hydrogen Energy 2015;40(30):9201–8. https://doi.org/10.1016/j.ijhydene.2015.05.147.
[38] Singh S, Bahari MB, Abdullah B, Phuong PTT, Truong QD, Vo D-VN, Adesina AA. Bi-reforming of methane on Ni/SBA-15 catalyst for syngas production: influence of feed composition. Int J Hydrogen Energy 2018;43(36):17230–43. https://doi.org/10.1016/j.ijhydene.2018.07.136.
[39] Ayodele BV, Khan MR, Lam SS, Cheng CK. Production of CO-rich hydrogen from methane dry reforming over lanthania-supported cobalt catalyst: kinetic and mechanistic studies. Int J Hydrogen Energy 2016;41(8):4603–15. https://doi.org/10.1016/j.ijhydene.2016.01.091.
[40] Abdollahifar M, Haghighi M, Sharifi M. Dry reforming of methane over nanostructured Co/Y catalyst for hydrogen production: effect of ultrasound irradiation and Co-loading on catalyst properties and performance. Energy Convers Manag 2015;103:1101–12. https://doi.org/10.1016/j.enconman.2015.04.053.
[41] Ayodele BV, Hossain SS, Lam SS, Osazuwa OU, Khan MR, Cheng CK. Syngas production from CO_2 reforming of methane over neodymium sesquioxide supported cobalt catalyst. J Nat Gas Sci Eng 2016;34:873–85. https://doi.org/10.1016/j.jngse.2016.07.059.
[42] Fayaz F, Bach LG, Bahari MB, Nguyen TD, Vu KB, Kanthasamy R, Samart C, Nguyen-Huy C, Vo D-VN. Stability evaluation of ethanol dry reforming on Lanthania-doped cobalt-based catalysts for hydrogen-rich syngas generation. Int J Energy Res 2019;43(1):405–16. https://doi.org/10.1002/er.4274.
[43] Nagaoka K, Okamura M, Aika K. Titania supported ruthenium as a coking-resistant catalyst for high pressure dry reforming of methane. Catal Commun 2001;2(8):255–60. https://doi.org/10.1016/S1566-7367(01)00043-7.
[44] Diallo A, Beye AC, Doyle TB, Park E, Maaza M. Green synthesis of Co_3O_4 nanoparticles via Aspalathus linearis: physical properties. Green Chem Lett Rev 2015;8(3-4):30–6. https://doi.org/10.1080/17518253.2015.1082646.
[45] Liu WW, Chai SP, Mohamed AR, Hashim U. Synthesis and characterization of graphene and carbon nanotubes: a review on the past and recent developments. J Ind Eng Chem 2014;20(4):1171–85. https://doi.org/10.1016/j.jiec.2013.08.028.
[46] Bharatish A, Murthy HNN, Aditya G, Anand B, Satyanarayana BS, Krishna M. Evaluation of thermal residual stresses in laser drilled alumina ceramics using Micro-Raman spectroscopy and COMSOL Multiphysics. Optic Laser Technol 2015;70:76–84. https://doi.org/10.1016/j.optlastec.2015.01.009.
[47] Zappa D, Bertuna A, Comini E, Molinari M, Poli N, Sberveglieri G. Tungsten oxide nanowires for chemical detection. Anal Methods 2015;7(5):2203–9. https://doi.org/10.1039/C4AY02637C.

Please cite this article as: Tran NT et al., Improvements in hydrogen production from methane dry reforming on filament-shaped mesoporous alumina-supported cobalt nanocatalyst, International Journal of Hydrogen Energy, https://doi.org/10.1016/j.ijhydene.2020.06.142